# Simulation Modeling of Kinematic Structures of Parallel Mechanisms

**Naqibullah Daneshjo**
Department of Marketing, Faculty of Commerce, University of Economics in Bratislava, Slovakia
daneshjo47@gmail.com

**Matej Scerba**
Department of Flight Training, Faculty of Aeronautics, Technical University of Kosice, Slovakia
matej.scerba@tuke.sk (corresponding author)

**Renata Sevcikova**
Department of Marketing, Faculty of Commerce, University of Economics in Bratislava, Slovakia
renata.sevcikova@euba.sk

**Samer Al-Rabeei**
Department of Aviation Engineering, Faculty of Aeronautics, Technical University of Kosice, Slovakia
samer.al-rabeei@tuke.sk

**Samuel Mir**
Department of Aviation Engineering, Faculty of Aeronautics, Technical University of Kosice, Slovakia
samuel.mir@tuke.sk

*Received: 10 December 2024 | Revised: 29 December 2024 | Accepted: 4 January 2025*

 *DOI: https://doi.org/10.48084/etasr.9898*

## ABSTRACT

**The present study offers an in-depth examination of the current advancements and the prevailing state of parallel kinematic structures, with a particular emphasis on Delta robots. The central focus of this study is the design solution of the Delta robot model in the Pro/ENGINEER system. The study explores the design and strength calculation of the individual components of the Delta robot, in addition to determining its workspace. Parallel mechanisms are distinguished by their unique kinematic structure, which is embodied by a closed kinematic chain. The terminal effector of the mechanism is then connected to the base by multiple arms. This configuration offers distinct advantages, primarily in terms of enhanced rigidity and related properties. The direct kinematic problem is employed to derive the coordinates of the end effector from the known positions of the actuators. While this task is not essential for the robot's movement per se, it is used during initialization and calibration, when the positions of the actuators are known, and the position of the end effector must be determined to move it to a specific location. The inverse kinematic problem, on the other hand, plays a critical role in continuous calculations during movement, as it transforms the world coordinates of the end effector into joint coordinates. This task is essential for robot control, as it enables the calculation of the positions of the individual actuators, given the desired position of the end effector.**

***Keywords-parallel kinematic structures; Delta robot; strength calculation***

## I. INTRODUCTION

In recent years, there has been an observable transfer of high-speed machining technologies, such as High-Speed Cutting (HSC), from research settings to engineering practice. This transition is driven by emerging trends that are generating new demands for robots and their applications. These demands are primarily related to the effective usage of robots in new areas of the non-manufacturing and service sectors. The evolution of robotics is being shaped by these factors, which are increasing the complexity of innovations across all resources involved in automated manufacturing and operational systems [1, 2]. This has led to a paradigm shift in the design of machine tools. The traditional concept of machines with long open kinematic chains, where the individual axes of motion are arranged sequentially—known as the serial kinematic structure

of machines—has become an impediment to achieving the necessary high speeds and accelerations of the machines' moving elements. Consequently, novel principles for the construction of machine tools have emerged, with a focus on closed parallel kinematic structures [3, 4]. The kinematic structure of manufacturing machines and industrial robots consists of various components that are connected by kinematic pairs and force elements. A kinematic pair is defined as a connection between two elements, each of which is movable, with the constraint that the motion of one element relative to the other is restricted. The configuration and arrangement of these kinematic pairs determine the workspace of the manufacturing machines and industrial robots. The assembly of kinematic pairs gives rise to the formation of a kinematic chain, as evidenced by several elements connected by these pairs [5]. The employment of parallel mechanisms is particularly advantageous in scenarios where alternative structures are inadequate or do not align with specific requirements [6, 7]. Devices based on parallel kinematic structures are increasingly gaining traction in various industries. In the domain of manipulation, robots equipped with parallel kinematic structures have become indispensable [8]. These mechanisms have been extensively used in research, particularly in the field of solar cell production, and have traditionally played a significant role in final processing and finishing operations, such as the food industry.

## II. DETERMINATION OF THE KINEMATIC SCHEME OF A DELTA ROBOT

The kinematic scheme of the Delta robot is based on the scheme of the Hexa robot, which has six Degrees of Freedom (DOF). In this scheme, individual chains are combined into pairs that share a common path, resulting in a mechanism with three DOF, as shown in Figure 1. The movable platform is connected to the base by three kinematic chains. Each chain consists of a rotational drive (R) and two pairs of spherical joints (SS). This configuration is referred to as 3-DOF 3-R(SS)(SS).

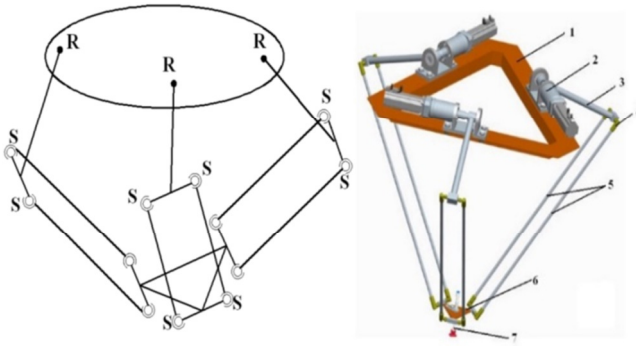


Fig. 1. Kinematic diagram and design proposal of the Delta robot: 1 – upper platform, 2 – drive subsystem, 3 – driving arm, 4 – spherical joint, 5 – driven arms, 6 – movable platform, 7 – vacuum gripper.

The configuration of the Delta robot is determined by the designated kinematic scheme, which stipulates the assembly of a three-dimensional model through the usage of the Pro/ENGINEER program. To ascertain the dimensions of its constituent parts, it is imperative to determine the torque necessary to articulate a single arm. This torque is then used to select the optimal type of drives, whose torque will be the primary determining parameter for sizing the individual components of the mechanism [9]. The upper platform constitutes the stationary component of the Delta robot and is composed of L-profiles of material 11 343, with dimensions of 40 × 60, in two lengths, and is cut at an angle of 60°, which will subsequently be welded together into a single unit. The lower platform constitutes the movable component of the Delta robot, exhibiting three degrees of mobility. The fabrication of this component involves the use of 5 mm steel of class 11 500. The end effector is attached to the lower platform.

## III. DESIGN OF JOINTS FOR CONNECTING THE DRIVE AND DRIVEN ARM

The design of the Delta robot in this study incorporates two alternative designs of universal joints, which collectively provide three degrees of motion for the movable platform.

### *A. The Equivalent of a Universal Joint*

The mechanism under consideration consists of spherical bearings and a sliding bearing. The kinematic scheme, as depicted in Figure 2, presents the rotation of the mechanism around two axes. The rotation around the x-axis is achieved through the engagement of the sliding bearing, while the rotation around the y-axis is enabled by the ball bearings, which are responsible for the movement of the driven arms.

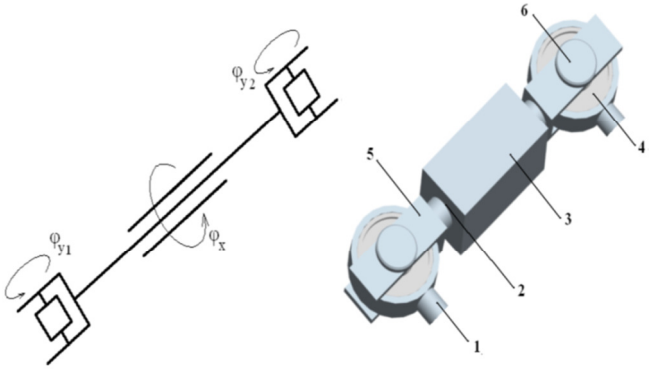


Fig. 2. Kinematic diagram and model of the universal joint: 1 – driven arm, 2 – sliding bearing, 3 – bearing arrangement, 4 – ball bearing, 5 – fork, 6 – retaining pin.

### *B. Spherical Joint*

The ball joint is composed of material BS. 970 230M 07Pb, which is defined as leaded low-carbon steel with a hardened surface and zinc plating. The inner support ring is composed of drawn steel SAE 1070, and the assembly in its entirety is lubricated with a specialized agent. This ball joint is well-suited for harsh conditions due to its resistance to wear and its ability to withstand vibrations and high impact loads. In comparison to the universal joint, it is notable for its reduced weight and its structural simplicity. The schematic of the spherical joint, with the corresponding dimensions are presented in Figure 3 and

Table I, respectively. Consequently, it was selected as the optimal solution for the Delta robot's design.

### *C. Selection of the Effector*

The selection of the effector is dependent on various factors, primarily the type of material, size, weight, and shape of the object being manipulated. Delta robots, in particular, use mechanical, vacuum, and magnetic effectors. For the Delta robot under consideration, a vacuum effector equipped with a flexible suction cup was selected on the basis of its cost-effectiveness, ease of maintenance, affordability, and adaptability to grasping diverse materials. The effector is firmly attached to the movable platform using a system of screws and nuts, as illustrated in Figure 4. It is hypothesized that the effector will be capable of handling objects with a flat upper surface, such as cylindrical shapes, made from different types of materials, with a maximum weight of up to 0.5 kilograms.

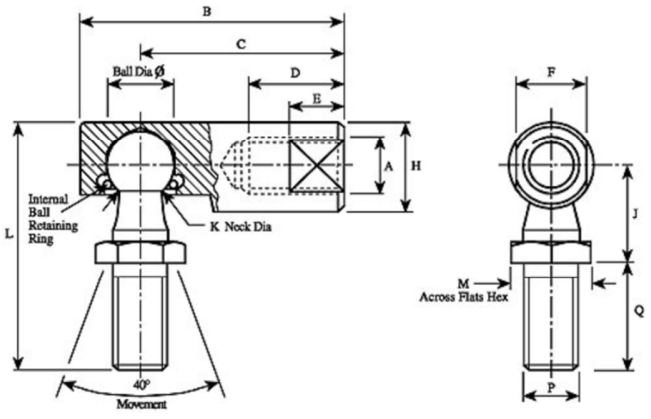


Fig. 3. Spherical joint with the corresponding dimensions.

TABLE I. DIMENSIONS OF THE SPHERE (MM)

| A | B | C | D | E | F | H | J | K | L | K | Q | Sphere diameter | Weight (100 pieces) |
|---|---|---|---|---|---|---|---|---|---|---|---|---|---|
| M6×1 | 31.4 | 24.6 | 12.7 | 7 | 9.5 | 11.5 | 11.9 | 5.52 | 31.7 | 10 | 14.2 | 7.75 | 2.3 kg |

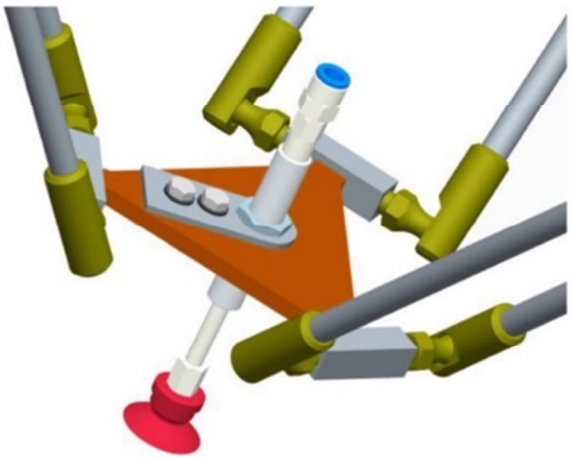

Fig. 4. Attachment of the accessory to the movable platform and method of grasping the handling object.

The suction cup model ZPT25CN-B01, featuring supporting ribbing, was selected from the SMC automation catalog and is composed of acrylo-Nitrile Butadiene Rubber (NBR) material, with a diameter of 25 millimeters.

### *D. Selection of Ejector*

The selection of the ejector is contingent upon the maximum vacuum pressure with which it operates. To ascertain the vacuum pressure ($p$) necessary to elevate the desired object, it is imperative to use:

$$p = \frac{Fs}{s} = \frac{k_p \times F}{S} = \frac{k_p \times m \times (g+a)}{\frac{\pi \times d^2}{4}} = \frac{0{,}5 \times 4 \times (9{,}81+1)}{\frac{\pi \times 0{,}025^2}{4}} = 33091Pa = 33kPa \quad (1)$$

where $F_S$ is the suction force, $F$ is the sum of gravitational and inertial forces of the manipulated object, $k_P$ is the safety factor for gripping, equal to 4, and $S$ is the area under the suction cup, as portrayed in Figure 5. The EZH 10BS-06-06 effector, selected from the SMC automation catalogue, has been designated for use in this application. The effector functions at a maximum vacuum pressure of 46 kPa.

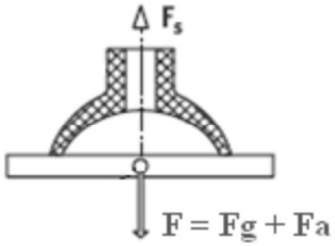


Fig. 5. Diagram showing the forces acting during the vertical lifting of the handling object.

## IV. CALCULATION OF THE TORQUE REQUIRED FOR ARM MOVEMENT

To calculate the torque, it is necessary to determine the approximate masses of the moving parts of the robot that are in the chain following the drive, towards the moving platform. Furthermore, the manipulated object attached to the moving platform will be considered. The maximum mass of the manipulated object is set to 0.5 kg, and the maximum acceleration of the Delta robot is a= 1 $ms^{-2}$.

### *A. Calculation of the Mass of Moving Components*

The present study is an expansion of an initial design of the Delta robot. The mass of components can be determined using the mass properties command in Pro/ENGINEER. The mass of the moving components is a crucial metric in the analysis: moving platform 0.15 kg, vacuum effector 0.2 kg, spherical joint 0.035 kg, driving arm 0.35 kg, driven arm 0.25 kg. Due to the complexity of the calculations, a simplified model situation has been chosen, in which the moving platform of the Delta robot moves vertically upward.

### *B. Static Equilibrium of Forces*

The inertial force $F_A$ and the gravitational force $F_G$ are divided by a factor of three because they are distributed among

the three arms, where the force $F_C$ that moves the platform is generated, as presented in Figure 6. The mass of the platform $m_1$, the effector, and the controlled object, is 0.85 kg.

$$\Sigma_{i=1}^{n} F_{iy} = 0 \quad F_{cy} - \frac{(Fg+Fa)}{3} = 0 \quad F_g = m_1 \times g \tag{2}$$

$$F_a = m_1 \times a \quad F_{cy} = \frac{m_1 \times (g+a)}{3} \tag{3}$$

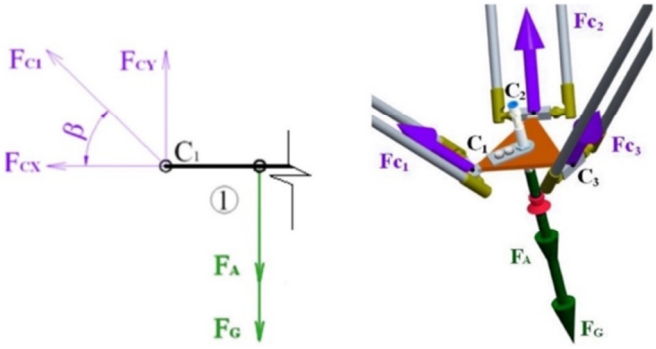


Fig. 6. Representation of the acting forces.

### C. Static Equilibrium on the Driven Arms

The arms are subjected to tensile forces acting at points B and C ($F_B$, $F_C$). In addition, the weight of the arms $F_{G2}$ is incorporated into the calculations. The mass of the driven arms, spherical joints, and connectors, denoted by $m_2$, is measured at 0.8 kg, as shown in Figure 7.

$$\Sigma_{i=1}^{n} F_{ix} = 0 \quad F_{cx} - F_{bx} = 0 \tag{4}$$

$$\Sigma_{i=1}^{n} F_{iy} = 0 \quad F_{By} - F_{Cy} - F_{G2} = 0 \quad F_{G2} = m_2 \times g \tag{5}$$

$$F_{By} = F_{Cy} + F_{G2} \tag{6}$$

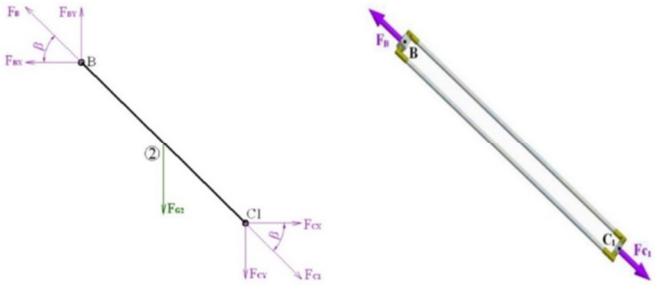


Fig. 7. Representation of the forces acting on the rod 2.

### D. Static Equilibrium on the Drive Arm

The tensile forces acting on the drive arm are:

$$\Sigma_{i=1}^{n} F_{ix} = 0, F_{Bx} - R_{Ax} = 0 \tag{7}$$

$$\Sigma_{i=1}^{n} F_{iy} = 0, R_{Ay} - F_{By} - F_{G3} = 0, F_{G3} = m_3 \times g \tag{8}$$

$$\Sigma_{i=1}^{n} M_{iA} = 0, \; M_A - F_{BM} \times l - F_{GM} \times \frac{l}{2} = 0 \tag{9}$$

$$M_A = F_{BM} \times l + F_{GM} \times \frac{l}{2}, F_{BM} \frac{F_{By}}{\cos\alpha}, F_{GM} = \frac{F_{G3}}{\cos\alpha} \tag{10}$$

$$M_A = \frac{\frac{m_1 \times (g+a)}{3} + m_2 \times g}{\cos\alpha} \times l + \frac{m_3 \times g}{\cos\alpha} \times \frac{l}{2} \tag{11}$$

where $M_A$ is the torque required for the movement of the entire system, $F_{BM}$ is the force component, $F_B$ is the torque inducing component, $F_{GM}$ is the force component, $F_{G3}$ is the torque inducing component, $R_{AX}, R_{AY}$ are the reactions on the drive shaft, $m_3$ is the mass of the drive arm equal to 0,35 kg, and $l$ is the lenght of the drive arm equal to 250 mm, as exhibited in Figure 8.

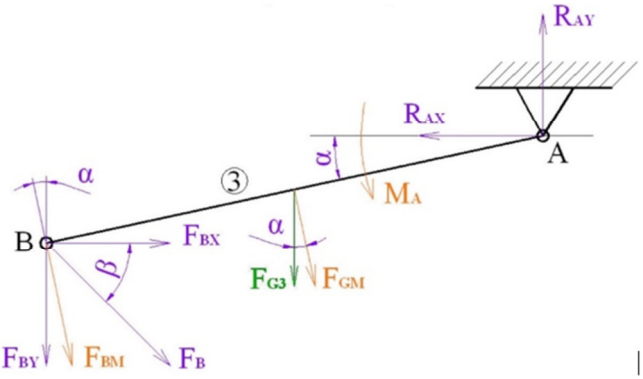


Fig. 8. Representation of the forces acting on the driving arm.

According to the established motion equations, the angle $\alpha$ exerts a significant influence on the magnitude of the torque, as displayed in Figure 9. The range of angle $\alpha$ for the Delta robot is determined by its design, varying from -40° to 75°. The maximum torque of 13.484 Nm is attained at an angle of $\alpha$=75°, as presented in Figures 9 and 10. A servomotor of the type Q1AA04010D, characterized by its low inertia, has been selected for the drive, manufactured by ALL Motion. In addition, a planetary gearbox from the same supplier, designated as the AE050-100 model, has been chosen for its optimal gear ratio in relation to the motor's torque, its low inertia, and its minimal backlash. These components have been selected from the catalog due to their technical specifications, which are deemed to be adequate for the intended application.

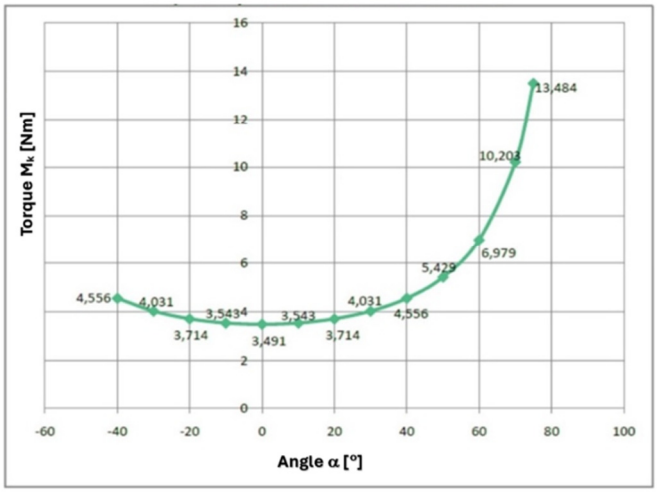


Fig. 9. Graph showing the dependence of angle $\alpha$ on torque.

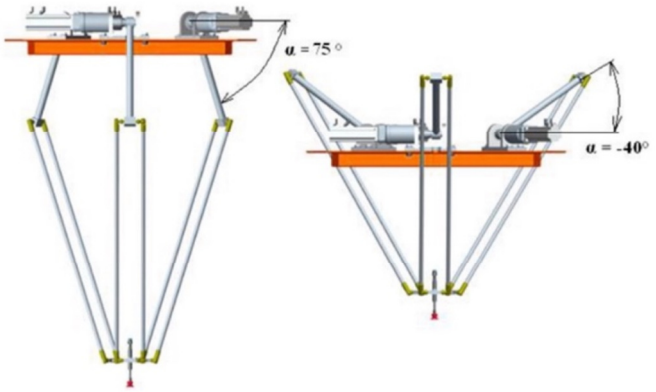


Fig. 10. Extreme working positions of the Delta robot during upward movement.

## V. DESIGN OF THE ARM SUPPORT PIN

The support shaft of the Delta robot is used for the purpose of transferring the torque from the gearbox shaft to the mobile components of the Delta robot. As evidenced in the diagram in Figure 11, the support shaft is subjected to combined loading, encompassing torsion and bending. Consequently, the calculations for its diameters are contingent on these two types of loads (or its reduced load). The connection between the arm's support shaft and the motor's output shaft is modeled as a connection that allows for rotation, rather than a fixed connection.

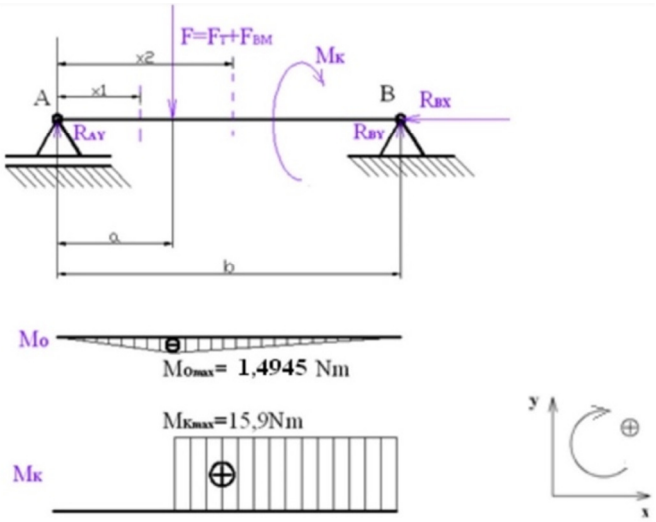


Fig. 11. Diagram of the loading of the supporting shaft.

In the diagram, $M_O$ is the bending moment, $M_K$ is the torsional moment, $F_T$ is the force of the arm's weight, $R_{BX}, R_{BY}$ are the reactions on the gearbox shaft, and $R_{AY}$ is the reaction generated at the bearing.

### A. Sum of Moments at Point B

If the aforementioned moments are summarized:

$$\Sigma_{i=1}^{n} M_{iB} = 0 \quad (12)$$

$$R_{Ay} \times b - (F_T + F_{BM}) \times (b - a) = 0 \quad (13)$$

$$R_{Ay} = \frac{F \times (b-a)}{b} = \frac{(63{,}6+20) \times (55-20)}{40} = 74{,}725\text{N} \quad (14)$$

### B. Calculation of Bending Moments

To calculate the bending, the theory of virtual cuts is employed:

$$M_{O1} = R_{Ay} \times x_1 \quad (15)$$

$$M_{O2} = R_{Ay} \times x_2 + F \times (x_2 - a) \quad (16)$$

To determine the bending diagram, it is necessary to calculate the value of $M_O$ at three points:

$$if\ x_1 = 0 \quad M_O = -74{,}725 \times 0 = O\ \text{Nm} \quad (17)$$

$$if\ x_2 = 20 \quad M_O = -74{,}725 \times 20 = 1{,}494.5\ \text{Nm} \quad (18)$$

$$if\ x_3 = 55 \quad M_{O2} = -74{,}725 \times 55 + 30 \times (55 - 20) = 0\ Nm \quad (19)$$

### C. Diameter Check (d) according to the HMH Theory

The relationship that combines the loading due to torsion and bending for material 11 500 is:

$$\sigma_{dov} = 100MPa \quad (20)$$

$$\sigma_{dov}^2 \geq \sigma_{0max}^2 + 3 \times \tau_{max}^2 \quad (21)$$

$$\sigma_{0max} = \frac{M_{0max}}{W_O} \quad \tau_{max} = \frac{M_{Kmax}}{W_K} \quad (22)$$

The section modulus for bending $W_O$ and for torsion $W_K$ is calculated as:

$$W_0 = \frac{\pi \times d^3}{32} \quad W_K = \frac{\pi \times d^3}{16} \quad (23)$$

$$\sigma_{dov}^2 \geq \left(\frac{M_{0max}}{\frac{\pi \times d^3}{32}}\right)^2 + 3 \times \left(\frac{M_{Kmax}}{\frac{\pi \times d^3}{16}}\right)^2 \quad (24)$$

$$d \geq \sqrt[6]{\frac{\left(\frac{M_{0max} \times 32}{\pi}\right)^2 + 3 \times \left(\frac{M_{Kmax} \times 16}{\pi}\right)^2}{\sigma_{dov}^2}} = \sqrt[6]{\frac{\left(\frac{1494{,}5 \times 32}{\pi}\right)^2 + 3 \times \left(\frac{15900 \times 16}{\pi}\right)^2}{100^2}} \geq 11{,}22\ \text{mm} \quad (25)$$

In order to facilitate the process of diameter calculation a simplified methodology is applied, whereby the inscribed circle $d$ is the sole parameter under consideration, as shown in Figure 12. The diameter of the support shaft (14,3 ≥ 11,22 mm), designated as $d$, meets the stipulated requirements for strength calculation.

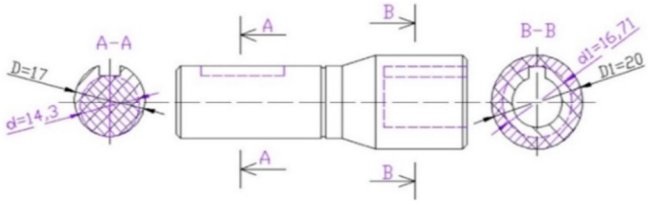


Fig. 12. The support shaft of the drive arm and its two dimensioned cross-sections.

*D. Strength Check of Diameters (D1,d1)*

In order to simplify the calculation, the inner diameter *d1*, which is formed by the fillet groove, is selected. In this calculation, the bending load is neglected. The parameter *D1* = 20 mm, and the permissible range is specified as:

$$\tau_{dov} = 55MPa, d1 = 16{,}71mm \quad (26)$$

$$\tau_{max} = \frac{M_{Kmax}}{W_K} \quad (27)$$

The section modulus for torsion $W_K$ for a tubular cross-section is calculated as:

$$W_K = \frac{\pi\times(D^4-d^4)}{16\times D} \quad (28)$$

$$\tau_{max} = \frac{M_{Kmax}}{\frac{\pi\times(D^4-d^4)}{16\times D}} = \frac{15900}{\frac{\pi(D^4-d^4)}{16\times D}} = 19{,}74 \quad (29)$$

$$\tau_{dov} \geq \tau_{max}\ , 55 \geq 19{,}74 \quad (30)$$

where $\sigma_{dov}$ is significantly higher than $\sigma_{max}$, therefore, the selected diameter of the support pin meets the strength requirements.

## VI. CHECK OF THE DRIVE ARM OF BENDING

The connection between the drive shaft and the gearbox shaft is replaced with a virtual fixed support, thereby restraining the shaft against movement. The force exerted at the end of the arm is the sum of the torque ($F_{BM}$) and the weight ($F_T$) of the remaining moving components, while the weight of the drive arm itself is negligible. The acceptable normal stress for the diminishing load of material 11500 is $\sigma_{dov}$= 100 MPa.

*A. Calculation of the Bending Moment*

The method of virtual cuts will be used:

$$M_O = (F_T + F_{BM}) \times x_1 \quad (31)$$

To determine the bending diagram, the value of $M_O$ at the endpoints will be calculated:

$$if\ x_1 = 0\ mm \quad M_O = -63{,}6 \times 0 = 0 \quad (32)$$

$$if\ x_2 = 250\ mm \quad M_O = -63{,}6 \times 250 = 15900\ Nm \quad (33)$$

*B. Strength Check*

$$\sigma_{max} = \frac{M_{Omax}}{W_O} \quad (34)$$

The section modulus for bending $W_O$ for a tubular cross-section is calculated as:

$$W_O = \frac{\pi\times(D^4-d^4)}{D\times 32} \quad (35)$$

$$\sigma_{max} = \frac{M_O}{\frac{\pi\times(D^4-d^4)}{D\times 32}} = \frac{15900}{\frac{\pi\times(18^4-14^4)}{18\times 32}} = 43{,}8\ MPa \quad (36)$$

$$\sigma_{dov} \geq \sigma_{max} \quad 100 \geq 43{,}8 \quad (37)$$

where $\sigma_{dov}$ is significantly higher than $\sigma_{max}$. Therefore, the selected diameter meets the strength requirements. Figures 13 and 14 display a 3D model and a diagram of the action of $F_{BM}$ on the driving arm.

## VII. CHECK OF THE DRIVEN ARM OF BUCKLING

In certain instances, the driven arm is subject to compression (e.g., during the inclined lifting of the moving platform). While the arm appears to meet the compressive requirements, its length necessitates the implementation of a buckling check. The modulus of elasticity in tension for steel class 11500 is $E$= 2×10$^5$ MPa. The proportional limit of the material of the rod, is designated by $\sigma_U$ = 335 MPa. The length of the rod, $l$, is set at 600 mm, while the constant, $n$, is determined based on the type of support for the rod ends, in this case $n$ = 1.

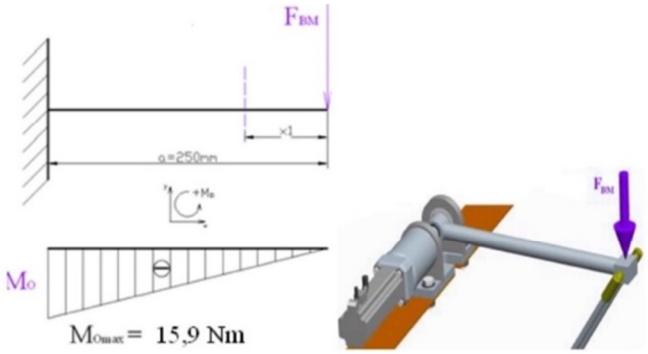


Fig. 13. Diagram and 3D model showing the action of the force $F_{BM}$ on the driving arm.


Fig. 14. Diagram of the force $F_{BM}$ acting on the driven arm.

*A. Quadratic Radius of the Cross-Section*

The following is a calculation of the quadratic radius of the cross-section:

$$i_{min} = \sqrt{\frac{Jmin}{A}} = \frac{\frac{\pi\times d^4}{64}}{\frac{\pi\times d^2}{4}} = \frac{d}{4} = \frac{8}{4} = 2\ mm \quad (38)$$

$$J_{min} = \frac{\pi\times d^4}{64}, A = \frac{\pi\times d^2}{4} \quad (39)$$

*B. Slenderness of the Rod*

The rod demonstrates a tendency toward slenderness:

$$\lambda = \frac{l}{i_{min}} = \frac{600}{2} = 300\ mm \quad (40)$$

and the way of limiting this slenderness is:

$$\lambda_m = \frac{\pi}{n} \times \sqrt{\frac{E}{\sigma_U}} = \frac{\pi}{1} \times \sqrt{\frac{2\times 10^5}{335}} = 76{,}76\ mm \quad (41)$$

*C. Determination of the Critical Force Using Euler's Formula*

Because $\lambda > \lambda_m$, Euler's formula can be used to determine the critical force:

$$F_{KR} = \frac{\pi^2 \times E \times J_{min}}{n^2 \times l^2} = \frac{\pi^2 \times 2 \times 10^5 \times 200{,}96}{1^2 \times 600^2} = 1102{,}45\ N \quad (42)$$

where the minimum principal central moment of inertia of the rod cross-section:

$$J_{min} = \frac{\pi \times d^4}{64} = \frac{\pi \times 8^4}{64} = 200{,}96\ mm^4 \quad (43)$$

A safety factor of $k = 5$ will be used, which modifies:

$$F \leq \frac{F_{KR}}{k} \quad 31{,}8 \leq 220{,}49 \quad (44)$$

The force $F = 31.8$ N acting on the rod is significantly less than $F_{KR}$, therefore the rod is in stable equilibrium. The approximate workspace of the Delta robot was assembled based on its structural parameters, using model situations in the Pro/ENGINEER program. The present work includes the design solution of the Delta robot model in the Pro/ENGINEER program, which will be further developed within the research of parallel kinematic structures. A significant portion of the research focuses on the design and sizing of the Delta robot's individual components, using fundamental static and strength equations. This approach also facilitates the estimation of the robot's approximate workspace, as presented in Figure 15.

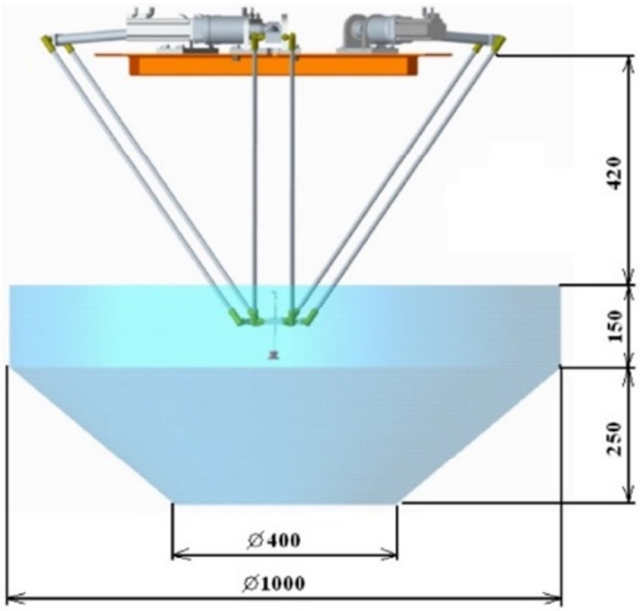


Fig. 15. Approximate workspace of the educational Delta robot.

## VIII. CONCLUSIONS

Parallel mechanisms have been demonstrated to be highly effective in practical applications and industrial production, particularly in the domains of handling and manufacturing devices. Recently, these mechanisms have garnered significant attention in the field of machining due to their remarkable dynamic capabilities at elevated platform speeds. The enhanced rigidity of their construction, attributable to their closed kinematic chain, underlies these advantages. Research on these structures has been conducted in university laboratories alongside research in the engineering industry [10, 11]. Despite the significant interest and investment in their development, the commercial success of parallel concepts remains limited [12,13]. Nevertheless, there is a strong inclination towards further development, as evidenced by the increasing frequency of conferences dedicated to this subject. Despite their recent emergence in the context of the long-standing tradition of classically designed machine tools, parallel mechanisms show promise for a promising future. Presently, their usage is confined to a specialized domain within the field of machining. As the design and construction of parallel mechanisms evolves, the selection of suitable applications for these machines becomes crucial. A particular emphasis has been placed on the selection of appropriate kinematic topologies for specific application tasks, with consideration for the development of modularity and the subsequent reconfiguration of these mechanisms. The advantages of parallel mechanisms, including enhanced dynamic properties and reduced stress on the structure, contribute to a reduction in energy consumption. Nevertheless, previous studies indicate that the creation of parallel mechanisms has not always been associated with a clear objective. Since their inception, these mechanisms have undergone a protracted development process. An analysis of machines with parallel kinematic structures has led to the conclusion that they are increasingly being used in industry, not only in the field of handling, but also in manufacturing.

## ACKNOWLEDGEMENT

This work has been supported by the Scientific Grant Agency of the Ministry of Education of the Slovak Republic (KEGA 003EU-4/2025 and VEGA 1/0064/23).

## REFERENCES

[1] S. Yang and Y. Li, "Kinematic analysis of deployable parallel mechanisms," *Proceedings of the Institution of Mechanical Engineers, Part C: Journal of Mechanical Engineering Science*, vol. 234, no. 1, pp. 263–272, Jan. 2020, https://doi.org/10.1177/0954406218825325.

[2] S. Pakzad, S. Akhbari, and M. Mahboubkhah, "Kinematic and dynamic analyses of a novel 4-DOF parallel mechanism," *Journal of the Brazilian Society of Mechanical Sciences and Engineering*, vol. 41, no. 12, Nov. 2019, Art. no. 561, https://doi.org/10.1007/s40430-019-2058-3.

[3] S. Liu, T. Huang, J. Mei, X. Zhao, P. Wang, and D. G. Chetwynd, "Optimal Design of a 4-DOF SCARA Type Parallel Robot Using Dynamic Performance Indices and Angular Constraints," *Journal of Mechanisms and Robotics*, vol. 4, no. 031005, Jul. 2012, https://doi.org/10.1115/1.4006743.

[4] S. Yang, T. Sun, and T. Huang, "Type synthesis of parallel mechanisms having 3T1R motion with variable rotational axis," *Mechanism and Machine Theory*, vol. 109, pp. 220–230, Mar. 2017, https://doi.org/10.1016/j.mechmachtheory.2016.11.005.

[5] Z. M. Bi and Y. Jin, "Kinematic modeling of Exechon parallel kinematic machine," *Robotics and Computer-Integrated Manufacturing*, vol. 27, no. 1, pp. 186–193, Feb. 2011, https://doi.org/10.1016/j.rcim.2010.07.006.

[6] L. Yang, X. Tian, Z. Li, F. Chai, and D. Dong, "Numerical simulation of calibration algorithm based on inverse kinematics of the parallel mechanism," *Optik*, vol. 182, pp. 555–564, Apr. 2019, https://doi.org/10.1016/j.ijleo.2019.01.079.

[7] T. A. Hess-Coelho, R. M. M. Orsino, and F. Malvezzi, "Modular modelling methodology applied to the dynamic analysis of parallel mechanisms," *Mechanism and Machine Theory*, vol. 161, Jul. 2021, Art. no. 104332, https://doi.org/10.1016/j.mechmachtheory.2021.104332.

[8] B. Dasgupta and P. Choudhury, "A general strategy based on the Newton–Euler approach for the dynamic formulation of parallel

manipulators," *Mechanism and Machine Theory*, vol. 34, no. 6, pp. 801–824, Aug. 1999, https://doi.org/10.1016/S0094-114X(98)00081-0.

[9] C. Della Santina, R. K. Katzschmann, A. Bicchi, and D. Rus, "Model-based dynamic feedback control of a planar soft robot: trajectory tracking and interaction with the environment," *The International Journal of Robotics Research*, vol. 39, no. 4, pp. 490–513, Mar. 2020, https://doi.org/10.1177/0278364919897292.

[10] S. Briot, V. Arakelian, and S. Guégan, "Design and Prototyping of a Partially Decoupled 4-DOF 3T1R Parallel Manipulator With High-Load Carrying Capacity," *Journal of Mechanical Design*, vol. 130, no. 12, Oct. 2008, Art. no. 122303, https://doi.org/10.1115/1.2991137.

[11] S. Staicu and D. Zhang, "A novel dynamic modelling approach for parallel mechanisms analysis," *Robotics and Computer-Integrated Manufacturing*, vol. 24, no. 1, pp. 167–172, Feb. 2008, https://doi.org/10.1016/j.rcim.2006.09.001.

[12] O. Altuzarra, M. Urizar, M. Cichella, and V. Petuya, "Kinematic Analysis of three degrees of freedom planar parallel continuum mechanisms," *Mechanism and Machine Theory*, vol. 185, Jul. 2023, Art. no. 105311, https://doi.org/10.1016/j.mechmachtheory.2023.105311.

[13] A. Alsaraira, K. Younes, S. Alabed, and O. Saraereh, "Wireless Controlled Robotic Hand using an LED-LDR Sensor," *Engineering, Technology & Applied Science Research*, vol. 14, no. 5, pp. 17046–17054, Oct. 2024, https://doi.org/10.48084/etasr.8507.